

Article

Small-Sample Battery Capacity Prediction Using a Multi-Feature Transfer Learning Framework

Xiaoming Lu ¹, Xianbin Yang ², Xinhong Wang ¹, Yu Shi ¹, Jing Wang ¹, Yiwen Yao ¹, Xuefeng Gao ¹, Haicheng Xie ² and Siyan Chen ^{2,3,*}

¹ Jilin State Power Economic and Technical Research Institute, Changchun 130022, China

² College of Automotive Engineering, Jilin University, Changchun 130022, China

³ State Key Laboratory of Automotive Chassis Integration and Bionic, Jilin University, Changchun 130022, China

* Correspondence: chensiyan1987@jlu.edu.cn

Abstract: The accurate prediction of lithium-ion battery capacity is crucial for the safe and efficient operation of battery systems. Although data-driven approaches have demonstrated effectiveness in lifetime prediction, the acquisition of lifecycle data for long-life lithium batteries remains a significant challenge, limiting prediction accuracy. Additionally, the varying degradation trends under different operating conditions further hinder the generalizability of existing methods. To address these challenges, we propose a Multi-feature Transfer Learning Framework (MF-TLF) for predicting battery capacity in small-sample scenarios across diverse operating conditions (different temperatures and C-rates). First, we introduce a multi-feature analysis method to extract comprehensive features that characterize battery aging. Second, we develop a transfer learning-based data-driven framework, which leverages pre-trained models trained on large datasets to achieve a strong prediction performance in data-scarce scenarios. Finally, the proposed method is validated using both experimental and open-access datasets. When trained on a small sample dataset, the predicted RMSE error consistently stays within 0.05 Ah. The experimental results highlight the effectiveness of MF-TLF in achieving high prediction accuracy, even with limited data.



Academic Editor: Pascal Venet

Received: 20 November 2024

Revised: 3 February 2025

Accepted: 5 February 2025

Published: 7 February 2025

Citation: Lu, X.; Yang, X.; Wang, X.; Shi, Y.; Wang, J.; Yao, Y.; Gao, X.; Xie, H.; Chen, S. Small-Sample Battery Capacity Prediction Using a Multi-Feature Transfer Learning Framework. *Batteries* **2025**, *11*, 62. <https://doi.org/10.3390/batteries11020062>

Copyright: © 2025 by the authors. Licensee MDPI, Basel, Switzerland. This article is an open access article distributed under the terms and conditions of the Creative Commons Attribution (CC BY) license (<https://creativecommons.org/licenses/by/4.0/>).

1. Introduction

Batteries are essential energy storage devices that play a critical role in ensuring the efficient and safe operation of systems, directly influencing equipment performance [1–3]. Among the various battery types, lithium-ion batteries (LIBs) have emerged as the preferred choice due to their high energy density, minimal temperature sensitivity, portability, long cycle life, and excellent safety characteristics. These advantages have led to LIBs' widespread use in applications such as wearable electronics and electric vehicles. However, extreme operating conditions can result in high-risk failure scenarios, including gas generation, electrode cracking, internal short circuits, and overcharging or discharging [4–6]. Inaccurate predictions of a battery's aging state can prevent health management systems from issuing timely warnings, leading to premature failures and, in some cases, catastrophic accidents [2,7].

The state of health (SOH) is a key metric for assessing the aging of LIBs, typically defined as the ratio of remaining capacity to initial capacity. While the capacity of a single cell decreases monotonically over time, accurately predicting battery capacity remains

challenging due to uncertainties in operating conditions and the complexity of aging mechanisms [8–10]. This has spurred significant research interest in methods for predicting battery capacity trajectories, which are primarily classified into model-based and machine learning approaches. Model-based approaches derive capacity estimates through coefficient calibration in analytical formulations of electrochemical deterioration, encompassing semi-empirical decay functions and hybrid phenomenological models. These approaches often use filtering algorithms like Kalman Filters [11] or Particle Filters [12] to identify model parameters and predict capacity. While these methods can operate online, their accuracy heavily depends on the degradation model's fidelity [13,14]. Additionally, achieving both high accuracy and generalizability under diverse conditions remains challenging.

In contrast, machine learning methods are mechanism-free and non-parametric, leveraging powerful nonlinear mapping capabilities. Traditional methods, such as support vector machines [15], relevance vector machines [16], and neural networks [17], initially offered acceptable predictions. With advancements in artificial intelligence, more sophisticated architectures like Long Short-Term Memory (LSTM) networks have shown an exceptional performance in predicting battery lifespan [18–21]. For instance, Zhang et al. [22] developed an SOH estimation method using incremental capacity (IC) and LSTM network; the MAPE of the estimation results was <2% for all the different battery samples. Similarly, Xu et al. [14] proposed a convolutional neural network-LSTM (CNN-LSTM) model to address the problem of neural network degradation caused by multi-layer LSTM; the RMSE was below 0.004 on the NASA dataset and the Oxford dataset. Zhao et al. [23] developed a hybrid attention and deep learning model integrating the strengths of the CNN, gated recurrent unit (GRU) recurrent neural network, and attention mechanism to forecast the battery's SOH; all the estimation errors could be maintained within 1.3% without extracting highly correlated health features. Bi-directional LSTM (BiLSTM) processes sequential data through dual temporal dependencies (chronological and reverse-chronological), achieving enhanced temporal resolution and the superior detection of hidden electrochemical dynamics in capacity fade trajectories when benchmarked against conventional unidirectional architectures. As a result, BiLSTM is increasingly replacing LSTM in recent studies. Li et al. [24] proposed a BiLSTM-Transformer model to estimate the SOH of lithium-ion batteries during the fast charging process. Zhang et al. [25] proposed a method for estimating the SOH of lithium-ion batteries based on multiphysics features and CNN-Enhanced Feature Combination-BiLSTM (CNN-EFC-BiLSTM). The above methods achieved outstanding predictive performance across various datasets.

Despite these advancements, the existing methods face several limitations. Many require over 25% of the battery's full lifecycle data for training, which hinders quick and robust predictions in real-time applications [26]. While some state-of-the-art approaches attempt to predict lifespan using data from early cycles, they often fail to validate performance under varying operational conditions, such as fluctuating temperatures or different charge/discharge rates [27,28]. Moreover, traditional machine learning models typically assume there are consistent distributions between training and testing datasets, which is unrealistic for batteries subjected to diverse and dynamic environments. Consequently, prediction accuracy is significantly affected by real-world variability, highlighting the need for models capable of generalizing across different operating conditions while using limited data [29].

Transfer learning (TL) has recently been introduced as a promising solution for battery SOH estimation [30,31]. By fine-tuning the parameters of pre-trained models, TL-based methods, such as those combining TL with LSTM or GRU, demonstrated improved SOH estimation. Yao et al. [32] proposed a deep TL method that uses partial segments of charging/discharging data for battery capacity estimation. Chen et al. [33] developed

a TL model based on the LSTM neural network to achieve the analysis of LIBs aging modes, using the experimental battery aging data as the source data and the aging data as the target data. Zhu et al. [34] developed a rapid cycle life assessment framework with TL, which substitutes predictions for a continuous test to obtain the end points and corresponding degradation trajectories. These TL-based methods exhibit an excellent performance. However, challenges remain: (a) most approaches assume consistent data distributions between training and testing, limiting their applicability under real-world variability; and (b) the existing methods often fail to achieve high prediction accuracy for large-scale datasets or extract deep representative features effectively. This underscores the importance of developing advanced frameworks for small-sample scenarios that extract meaningful features of battery aging and maintain a robust prediction performance across varied conditions.

To address these gaps, this study proposes a multi-feature transfer learning framework (MF-TLF) for LIBs capacity predictions. The main contributions of this work are as follows:

1. A multi-feature analysis method is developed to comprehensively extract battery aging features, incorporating parameters such as voltage, current, and temperature.
2. The framework achieves early degradation trajectory prediction and accurate cross-domain predictions using only 10% of the training data after adequate pre-training.
3. A novel hybrid CNN-BiLSTM method is proposed, combining strong feature extraction capabilities with suitability for time-series processing.
4. Extensive validation is conducted on both proprietary multi-temperature datasets and publicly available datasets, demonstrating the model's generalizability.

2. Experiment and Feature Analysis

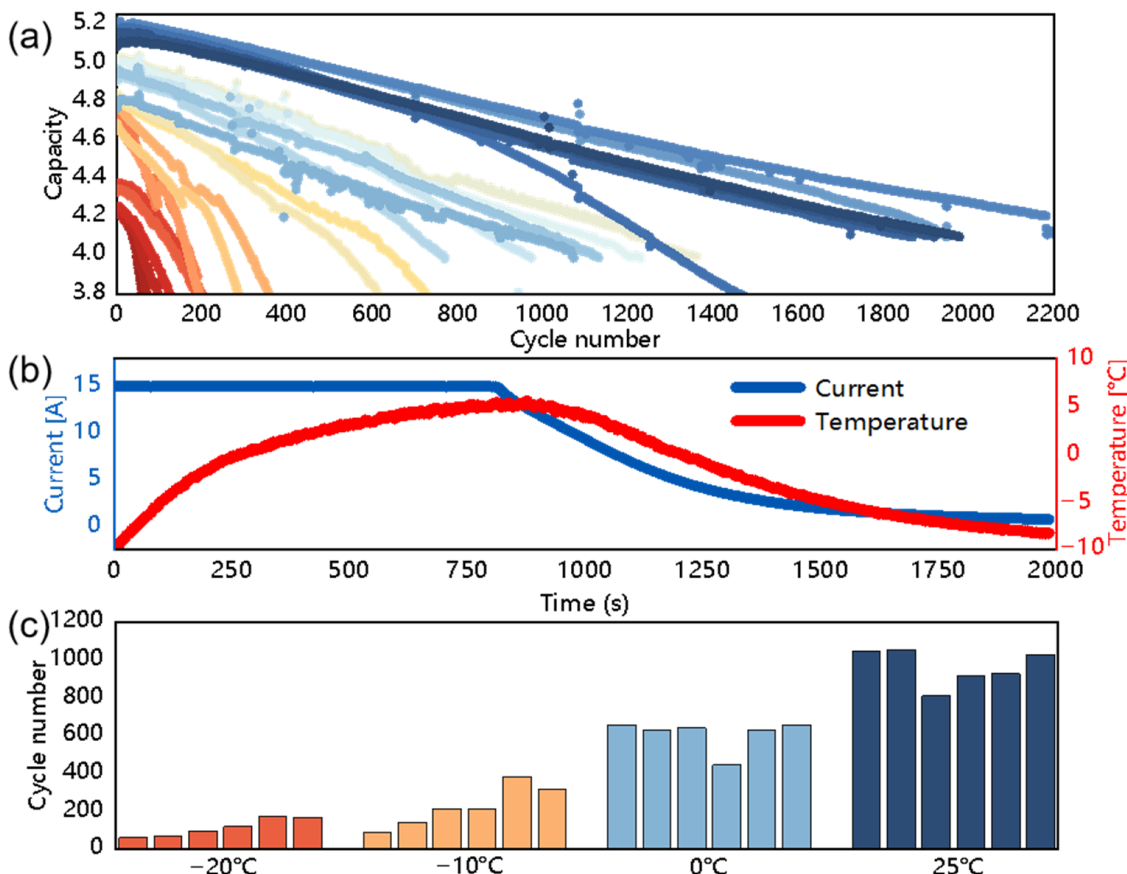
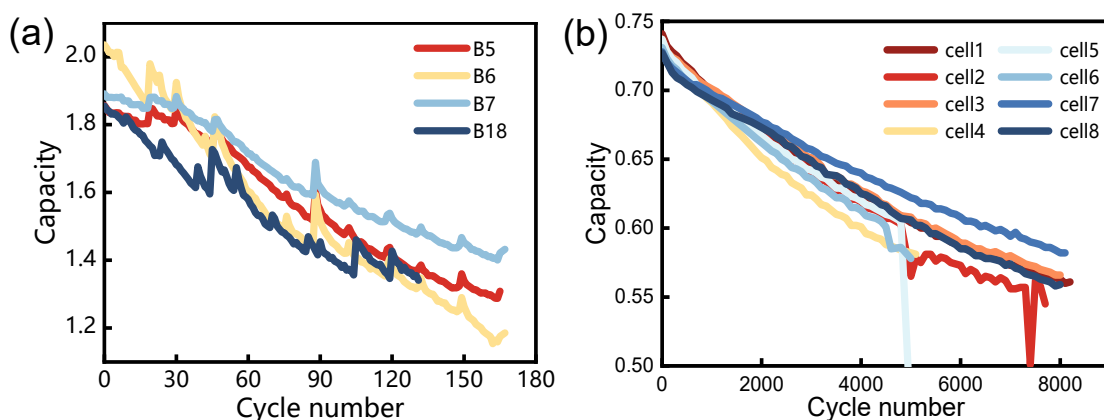
2.1. Related Data

We conducted aging experiments on 24 identical LIBs under varying operating conditions. Figure 1a shows the capacity decay trajectories of these cells across cycles, highlighting significant variations in degradation trends under different conditions. When operating conditions were identical, discrepancies in capacity decay were observed, attributed to the inherent inconsistencies among batteries [35]. These variations present challenges for the generalization of capacity prediction models. The experiments were conducted under multiple temperature conditions, all using high charge–discharge rates. Detailed experimental parameters are summarized in Table 1. Figure 2b illustrates the temperature and current profiles for a single charge–discharge cycle of a battery at $-10\text{ }^{\circ}\text{C}$, charged at a 3C rate.

At different temperatures, the batteries' initial capacities varied significantly. For example, in cold environments ($-20\text{ }^{\circ}\text{C}$ and $-10\text{ }^{\circ}\text{C}$), the capacity was noticeably lower than the nominal 5Ah, delivering approximately 4.3 Ah. This reduction is attributed to slowed lithium-ion diffusion kinetics, especially a significant decrease in solid-state diffusion rates, which obstructs the rapid insertion of lithium ions into the electrode materials [36]. This results in considerable voltage drops during battery discharging and premature termination of the battery cycle. To address this, a constant-voltage (CV) discharge step was incorporated during low-temperature aging cycles to ensure adequate lithium-ion intercalation/extraction in the electrodes and to maintain the charge–discharge depth. The cut-off current of the CV discharge step was 750 mA. Capacity measurements in this study were based on the CC-CV discharge values recorded during each cycle. Initial capacity benchmarks were established at $25\text{ }^{\circ}\text{C}$ and at each test temperature. At $25\text{ }^{\circ}\text{C}$, the initial capacity exceeded the nominal 5000 mAh, whereas capacities decreased significantly at lower temperatures due to the additional CV discharge step.

Table 1. Experimental pouch LIBs' parameters.

| LIB Chemistry | Nominal Capacity | Standard Charge/Discharge Current | Standard Discharge Current | Voltage Range | Maximum Charge/Discharge Current |
|-----------------|------------------|-----------------------------------|----------------------------|---------------|----------------------------------|
| NCM—hard carbon | 5000 mAh | 3C (15 A) | 3C (15 A) | 2.8 V–4.2 V | 10C (50 A) |

**Figure 1.** Experimental results: (a) battery degradation curves. The color of each curve represents a battery cell; (b) operating conditions for charging a cell at $-10\text{ }^{\circ}\text{C}$; (c) number of cycles for batteries to degrade to 90% SOH under different temperatures.**Figure 2.** Capacity trajectories: (a) NASA dataset; (b) Oxford dataset.

Operating conditions such as ambient temperature and charging current rates are recognized to impact the trajectories of battery aging. Figure 1c depicts the number of cycles needed for the batteries to reach 90% SOH degradation under varying conditions. Aging was observed to accelerate at lower temperatures due to decreased lithium-ion diffusion rates. At low temperatures during charging, lithium-ions are unable to promptly intercalate into the solid phase of the anode, leading to overpotential and the precipitation of metallic lithium. This phenomenon results in the depletion of a substantial portion of the lithium inventory, resulting in rapid capacity decay [37].

Additionally, two public datasets with distinct charge–discharge configurations, ambient temperatures, and battery chemistries were analyzed for comparison. The first dataset, the NASA dataset, includes aging experiments where batteries were charged at a constant current of 1.5 A until reaching a voltage of 4.2 V, followed by CV charging until the current dropped to 20 mA. Batteries B5, B6, B7, and B18 were discharged at CC of 2 A until terminal voltages of 2.7 V, 2.5 V, 2.2 V, and 2.5 V, respectively. As shown in Figure 2a, capacity degradation in this dataset exhibits recovery trends instead of a monotonic decline, complicating prediction efforts. This capacity rebound, which contrasts with typical decay patterns, presents a significant challenge for the predictive models. The second dataset, the Oxford dataset, includes data from cells labeled 1–8, each with a nominal capacity of 740 mAh. These experiments were conducted at a constant temperature of 40 °C. The cells were charged with a 2C current and discharged under dynamic conditions that simulate driving cycles. Every 100 cycles, 1C constant current charge/discharge cycles were conducted to measure the capacity. The capacity degradation trajectories of these cells are shown in Figure 2b. Differences in battery chemistry and operating conditions for the three datasets are shown in Table 2.

Table 2. Comparison of the three datasets.

| Dataset | Experimental | NASA | | | Oxford |
|---------------------------------|--------------------|-------|-------|-------|---------------------|
| Labels | - | B5 | B6 | B7 | B18 |
| Battery chemistry | NCM | | NCA | | Cell 1–8 LCO/NCO |
| Temperature [°C] | −20, −10, 0 and 25 | 24 | 24 | 24 | 40 |
| Nominal capacity [Ah] | 5 | 2 | 2 | 2 | 0.74 |
| Charging cut-off voltage [V] | 4.2 | 4.2 | 4.2 | 4.2 | 4.2 |
| Discharging cut-off voltage [V] | 2.8 | 2.7 | 2.5 | 2.2 | 2.7 |
| Standard Charging rate | 3C | 0.75C | 0.75C | 0.75C | 1C |
| Standard discharging rate | 3C | 1C | 1C | 1C | 1C |

2.2. Multi-Feature Analysis

LIBs exhibit complex performance characteristics under diverse operating conditions, making it difficult for a single feature to fully represent their SOH. To address this limitation, we employed a multi-feature analysis approach, extracting internal battery information from perspectives such as temperature, voltage, and current. This approach enhances the model's generalization ability, enabling it to better adapt to various usage scenarios [38]. One feature extraction method that was employed is Differential Thermal Voltammetry (DTV), which provides temperature-related insights. The DTV is defined as follows:

$$DTV = \frac{dT/dt}{dV/dt} = \frac{dT}{dV} \quad (1)$$

where T represents the surface temperature of the battery, V is the terminal voltage, and t is the sampling time. DTV is a diagnostic tool that offers direct insights into a battery's entropy behavior and is highly sensitive to degradation. Figure 3a illustrates the evolution

of DTV curves over cycling. Notable features include two prominent peaks near 3.45 V and 3.81 V and a distinct trough near 3.65 V. As cycling progresses, the peaks and troughs shift leftward, with the peaks showing decreasing DTV values and the trough demonstrating an increasing trend. These changes reflect the integration of voltage plateau shifts and material phase transition information into the DTV curves.

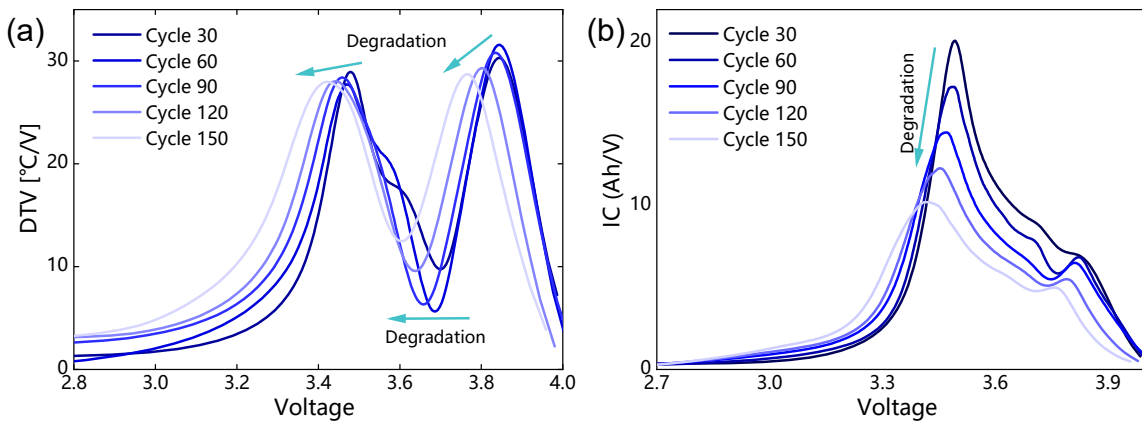


Figure 3. LIBs feature curves analysis: (a) evolution of DTV; (b) evolution of IC.

Another essential feature analysis method utilized is Incremental Capacity Analysis (IC), calculated as follows:

$$\frac{dQ}{dV} = \frac{I \times dt}{dV} = I \times \frac{dt}{dV} \quad (2)$$

where Q , I , V , and t represent discharge capacity, discharge current, battery voltage, and battery operating time, respectively. Traditional methods for analyzing charge–discharge voltage curves struggle to identify the start and end points of the voltage plateau due to the minimal numerical variation. This complicates the direct analysis of the battery's internal electrochemical reactions. In contrast, the IC curve, which is the reciprocal of the voltage change rate, intuitively represents the development of the voltage plateau and links external battery characteristics to internal electrochemical performance. As shown in Figure 3b, the positions and heights of peaks representing the voltage plateau decrease over time, with the peaks shifting leftward, indicating the downward movement of the voltage plateau as the battery ages.

During the computation of DTV and IC curves, noise in the measured temperature, current, and voltage introduces undesired variations, impacting feature extraction. To address this, the Savitzky–Golay (SG) filtering method was applied to smooth the IC curves. While DTV and IC effectively describe battery aging, their calculations involve differentiation and filtering, which are computationally intensive. Additionally, these methods are discharge-dependent, but discharge behaviors are influenced by unpredictable load profiles, with discharging currents fluctuating due to external demands. This randomness limits the practical utility of discharge-based features for capacity prediction.

To address this limitation, we propose a simpler feature extraction method based on the charging process, which is more stable and can be actively controlled by the Battery Management System (BMS), in contrast to discharge data, which are often constrained by user driving conditions [39]. Figure 4a highlights the evolution of voltage curves during aging, illustrating their rich degradation information. Figure 4b shows the typical CC-CV charging curve. We extract the charging time within a specific voltage range, defined as follows:

$$CTV(V_2, V_1) = CTV_2 - CTV_1 \quad (3)$$

where CTV represents the charging time at a given voltage. To balance data collection efficiency and the relevance of the collected data, we selected a CTV in the 3.8 V–3.9 V range as a key feature for SOH analysis. This voltage range corresponds to the mid-stage of charging, where voltage changes are relatively stable, enabling the consistent measurement of time differences between cycles.

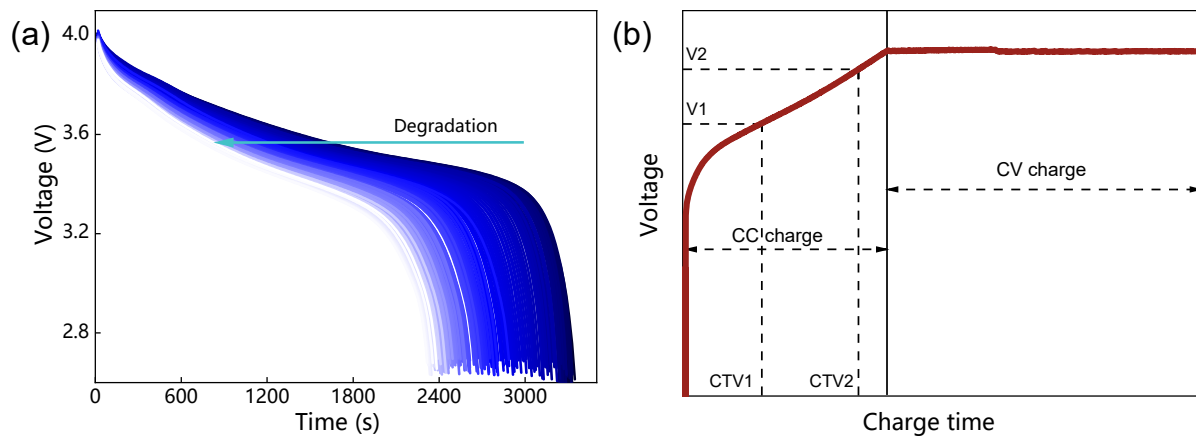


Figure 4. LIBs voltage of NASA B5: (a) evolution of voltage with degradation, different colors represent different cycles; (b) schematic of feature extraction.

3. Deep Learning Approach

We developed a deep learning framework for predicting the capacity of LIBs using transfer learning (TL). As shown in Figure 5, the framework incorporates a CNN-BiLSTM block, a temporal attention (TA) mechanism to enhance temporal feature focus, and Bayesian Optimization (BO) for efficient hyperparameter tuning. The training process is divided into two stages: pretraining and fine-tuning.

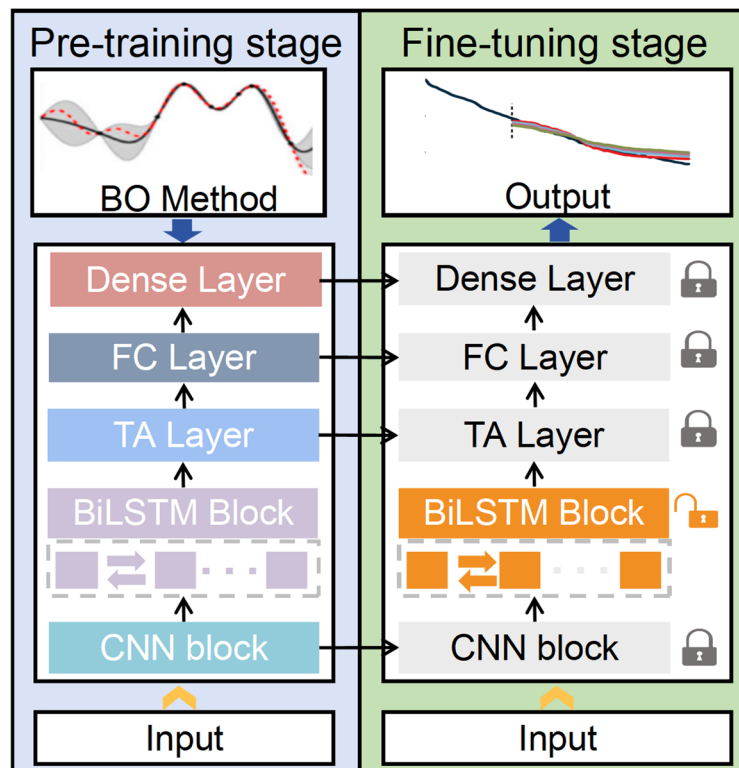


Figure 5. Deep learning method flowchart.

3.1. CNN and BiLSTM Block

CNNs are effective at extracting complex spatial features. In this framework, CNNs process raw time-series data, identifying and weighing the importance of critical features, which enhances the prediction performance. These features are then passed to a BiLSTM layer for deeper temporal analysis. A max-pooling strategy is employed to extract significant features and reduce computational complexity.

LSTM networks excel at capturing long-term dependencies in sequential data, making them well-suited for modeling the temporal evolution of battery degradation. Each LSTM unit comprises three gates (input, forget, and output) along with a cell state. These components work in unison to manage and regulate the flow of information through the network, ensuring that relevant data are retained or discarded at each time step. The forget gate removes irrelevant information from the previous state:

$$f_t = \sigma(W_{fx}x_t + W_{fh}h_{t-1} + b_f) \quad (4)$$

where x_t denotes the current input, h_{t-1} is the previous hidden state, W_{fx} and W_{fh} are the weight matrices for the forget gate, and $\sigma(\cdot)$ is the sigmoid activation function. The bias term is denoted by b_f , and f_t represents the output of the forget gate.

The input gate processes both the current input and the previous hidden state to create the candidate cell state, which represents potential updates to the cell's memory:

$$i_t = \sigma(W_{ix}x_t + W_{iH}h_{t-1} + b_i) \quad (5)$$

$$g_t = \tanh(W_{gx}x_t + W_{gH}h_{t-1} + b_g) \quad (6)$$

where W_{ix} and W_{iH} are the weight matrices for the input gate; W_{gx} and W_{gH} correspond to the candidate gate's weights. The $\tanh(\cdot)$ function is used for the candidate state, while b_i and b_g represent the biases for the input and candidate gates. The output of the input gate is given by i_t .

The cell state is updated by merging the forget and input gate outputs:

$$c_t = c_{t-1}f_t + i_tg_t \quad (7)$$

The output gate regulates the next hidden state by selecting which information from the cell state should be exposed as the output at the current time step:

$$o_t = \sigma(W_{ox}x_t + W_{oH}h_{t-1} + b_o) \quad (8)$$

$$h_t = o_t \tanh(c_t) \quad (9)$$

where W_{ox} and W_{oH} are the weight of the output gate, b_o is the bias of the output gate, o_t is the output gate activation, and h_t is the LSTM output.

The BiLSTM architecture comprises two LSTM layers, enabling the bidirectional processing of sequences. The predictions from both the forward and backward layers are combined and then passed through the subsequent layers for further processing and refinement. This bidirectional design improves the model's ability to capture dependencies in the CNN-extracted data, enhancing the accuracy of capacity trajectory predictions.

3.2. Temporal Attention Layer

While the BiLSTM layer captures sequential dependencies, not all past states contribute equally to the final capacity prediction. To emphasize the most relevant time points, we incorporated a temporal attention (TA) mechanism, which selectively weighs the im-

portance of different time steps. The TA layer dynamically assigns importance weights to hidden states across the time series.

The attention weight β_t for the hidden state h_t is computed as follows:

$$\beta_t = \frac{\exp(u_t)}{\sum_{i=1}^T \exp(u_i)} \quad (10)$$

$$u_t = v^T \tanh(W h_t + b) \quad (11)$$

where W and b are learnable parameters, v is a weight vector, and t is the total number of time steps. By emphasizing the most relevant hidden states, the TA layer improves both prediction accuracy and the interpretability of battery capacity trajectory estimation.

3.3. Transfer Learning

Accurate capacity prediction requires deep learning models trained on large datasets that reflect diverse battery aging scenarios. However, variations in operating conditions, such as temperature and charging protocols, create domain gaps between the training data (source domain) and the target operating environment (target domain). These gaps reduce the prediction accuracy.

TL mitigates this issue by leveraging knowledge from a data-rich source domain. The TL framework involves (a) pretraining the model on the source domain dataset and (b) fine-tuning the model with limited target domain data to adapt to specific degradation patterns.

During fine-tuning, only the BiLSTM parameters are retrained to align with the target domain's data, minimizing computational complexity. This selective adjustment enables the model to adapt to various battery chemistries and operating conditions, even with limited data.

In the pretraining phase, BO is employed to optimize hyperparameters. BO uses Gaussian processes to model the objective function, intelligently sampling promising hyperparameter configurations while avoiding suboptimal settings. This approach ensures efficient convergence to optimal parameters, reducing overfitting and enhancing generalization. The parameter ranges used for BO are listed in Table 3.

Table 3. Configurations of the hyper-parameter range.

| Hyper-Parameters | Selection Range |
|------------------|----------------------------|
| Learning rate | $(1 \times 10^{-4}, 0.01)$ |
| LSTM unit 1 | (16, 256) |
| LSTM unit 2 | (16, 256) |
| Dropout rate 1 | (0.1, 0.8) |
| Dropout rate 2 | (0.1, 0.8) |
| Loss function | MSE |
| Optimizer | Adam |

4. Results and Discussion

4.1. Results of Feature Analysis

To account for the complexity of capacity degradation caused by varied input conditions, we first analyzed the correlation between ten selected features and capacity degradation. The Pearson Correlation Coefficient (PCC), a widely used metric for measuring linear relationships, was employed to quantify the correlations.

The PCC between two variables, X and Y , is defined as follows:

$$\rho_{xy} = \frac{\sum_{i=1}^n (x_i - \bar{x})(y_i - \bar{y})}{\sqrt{\sum_{i=1}^n (x_i - \bar{x})^2} \sqrt{\sum_{i=1}^n (y_i - \bar{y})^2}} \quad (12)$$

where \bar{x} and \bar{y} represent the means of the feature values and LIB capacity, respectively; n denotes the sample size. The correlation coefficient ρ_{xy} ranges from -1 to 1 , where values closer to 1 or -1 indicate a stronger relationship, and values closer to 0 indicate a weaker relationship.

Figure 6 shows the correlation coefficients between features extracted using various methods and the battery capacity. Features derived from DTV analysis, IC analysis, and the CTV method exhibit high correlation coefficients, suggesting their effectiveness in capturing battery aging characteristics. Consequently, seven features with correlation coefficients greater than 0.8 were chosen as input variables for predicting battery capacity.

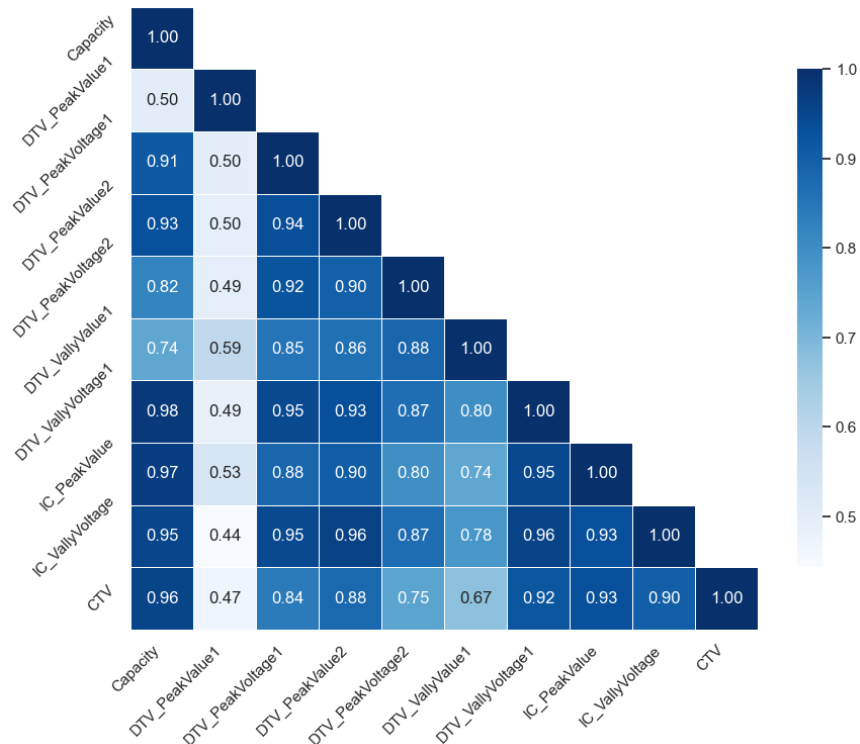


Figure 6. Correlation coefficients from multi-feature analysis.

4.2. Performance on Small Sample Prediction

Extensive experiments were conducted to validate the proposed model's performance across different datasets and operational conditions, including variations in temperature, battery chemistry, and C-rates. The NASA dataset, characterized by generalized conditions (low-rate and room-temperature), was used for pretraining. For fine-tuning, the first 10% of the target cell data was utilized to evaluate the model's small-sample prediction capability. During this phase, only the BiLSTM module parameters were fine-tuned.

Figure 7 displays the model's prediction results, with each subplot showing all experimental battery cells corresponding to a specific temperature condition. The proposed model achieved an excellent performance in small-sample predictions, with RMSE values below 0.05 Ah across all conditions. This result confirms the effectiveness of the chosen degradation features and demonstrates the robustness of the model training.

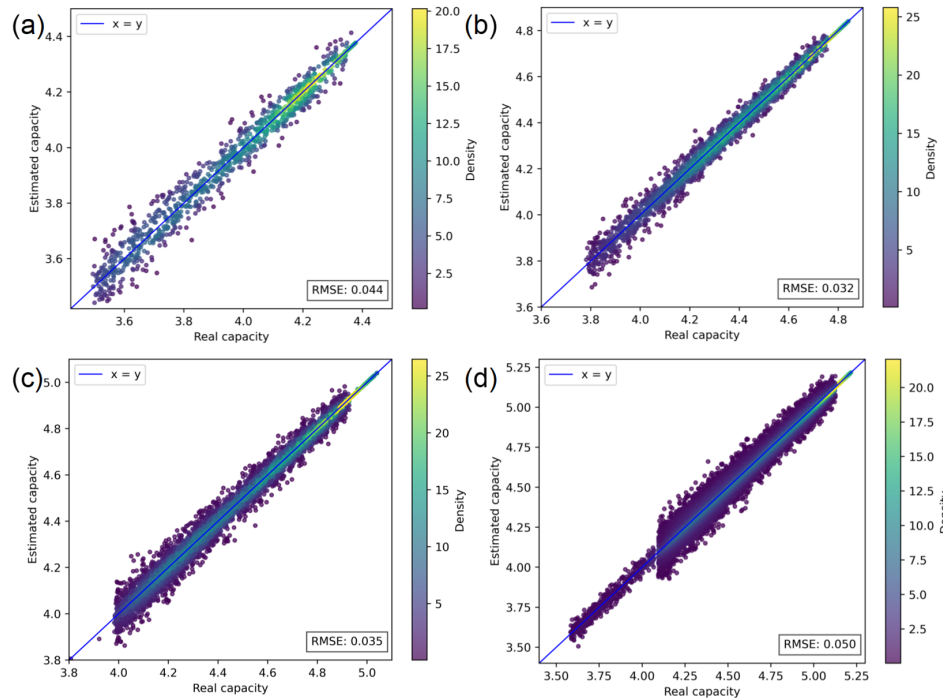


Figure 7. Performance on the experimental dataset using only the first 10% of data as the training set: (a) $-20\text{ }^{\circ}\text{C}$; (b) $-10\text{ }^{\circ}\text{C}$; (c) $0\text{ }^{\circ}\text{C}$; (d) $25\text{ }^{\circ}\text{C}$.

At $-10\text{ }^{\circ}\text{C}$, the model achieved the best performance, with an RMSE of 0.032 Ah, likely due to the distinct and consistent aging patterns at low temperatures, which provide clearer learning signals. Conversely, the model performed worst at $25\text{ }^{\circ}\text{C}$, with an RMSE of 0.050 Ah, potentially due to the complex and slower aging patterns at room temperature, as well as the increased data diversity in this condition, which may have increased training complexity.

Notably, the model maintained high accuracy even under extreme conditions, demonstrating its strong generalization capability in small-sample scenarios. This validates both the feature selection method and the fine-tuning strategy based on the BiLSTM module for capacity degradation prediction. To further evaluate the model's generalization, similar experiments were conducted on the Oxford dataset (Figure 8). Despite differences in battery chemistry and operating conditions, the model achieved an RMSE of 0.025 Ah. However, the predictions slightly exceeded the reference line, possibly reflecting deviations in the aging trends of the batteries in the dataset or the influence of differing battery chemistries on parameter adjustments.

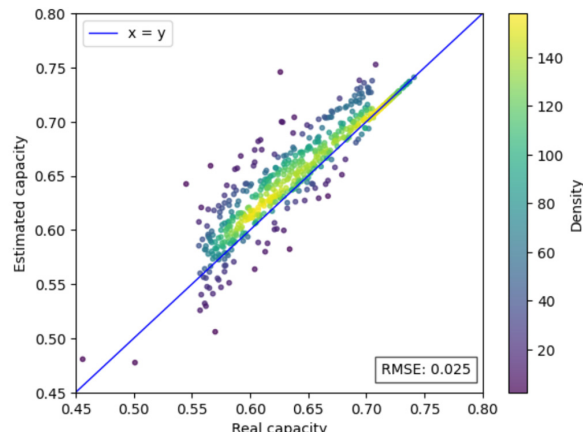


Figure 8. Performance on the Oxford dataset using only the first 10% of data.

4.3. Performance of Different Features

To comprehensively assess the proposed multi-feature fusion method and feature extraction strategies, we conducted comparative experiments (Figure 9) by selecting one representative cell per temperature condition, followed by systematic error analyses using box plots (Figure 10). The box represents the interquartile range. Points outside the whiskers are considered outliers, highlighting extreme values in the data. Table 4 summarizes the key results. The results show that while individual feature extraction methods can capture certain aging patterns, they are limited in handling complex conditions and diverse data. The multi-feature fusion method significantly improved prediction performance, achieving optimal results across all conditions. This indicates that the fusion method effectively combines the strengths of different features, providing a more comprehensive representation of battery aging characteristics.

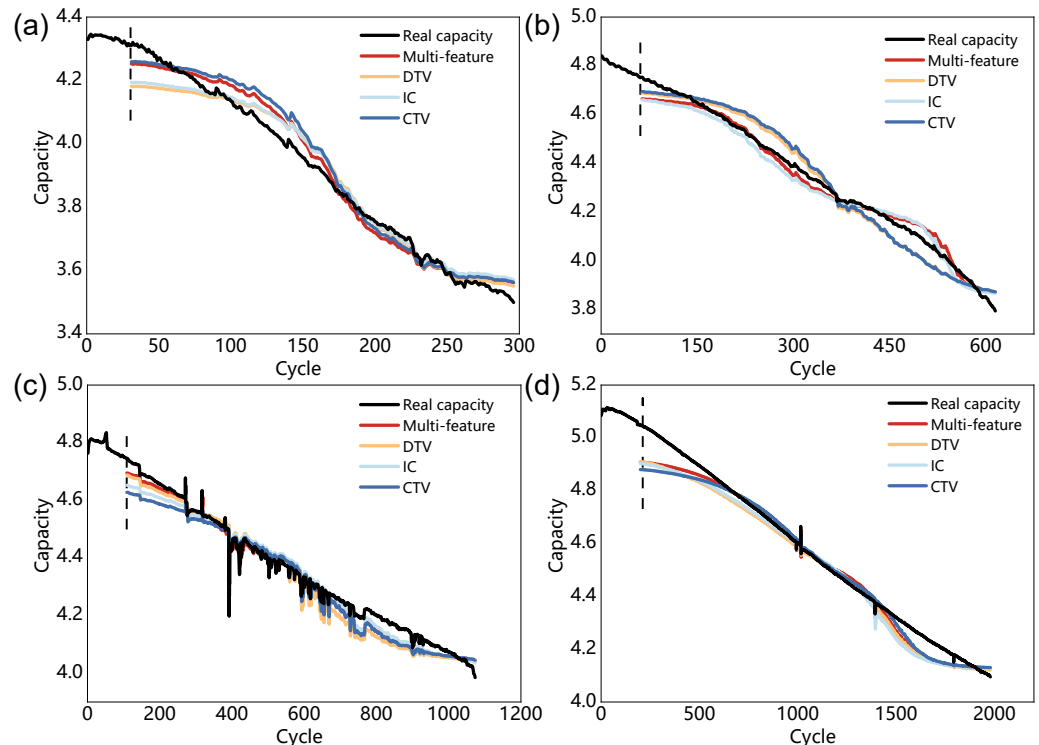


Figure 9. Comparison of different feature extraction methods on the experimental dataset, the dotted line indicates the cut-off point for the 10% cycle data: (a) $-20\text{ }^{\circ}\text{C}$; (b) $-10\text{ }^{\circ}\text{C}$; (c) $0\text{ }^{\circ}\text{C}$; (d) $25\text{ }^{\circ}\text{C}$.

Table 4. RMSE results of different feature methods.

| Condition | $-20\text{ }^{\circ}\text{C}$ | $-10\text{ }^{\circ}\text{C}$ | $0\text{ }^{\circ}\text{C}$ | $25\text{ }^{\circ}\text{C}$ |
|---------------|-------------------------------|-------------------------------|-----------------------------|------------------------------|
| Multi-feature | 0.038 | 0.033 | 0.032 | 0.048 |
| DTV | 0.048 | 0.052 | 0.042 | 0.056 |
| IC | 0.045 | 0.041 | 0.035 | 0.058 |
| CTV | 0.047 | 0.057 | 0.045 | 0.055 |

The CTV method exhibited the poorest performance under the $-10\text{ }^{\circ}\text{C}$ and $0\text{ }^{\circ}\text{C}$ conditions, likely due to its simplicity and reliance on a single feature, leading to incomplete information capture. Similarly, the DTV method performed worst under the $-20\text{ }^{\circ}\text{C}$ and $25\text{ }^{\circ}\text{C}$ conditions, potentially due to temperature-specific limitations. Although performance varied slightly among the different methods, all demonstrated good overall effectiveness, reinforcing the broad applicability and robustness of the proposed approach.

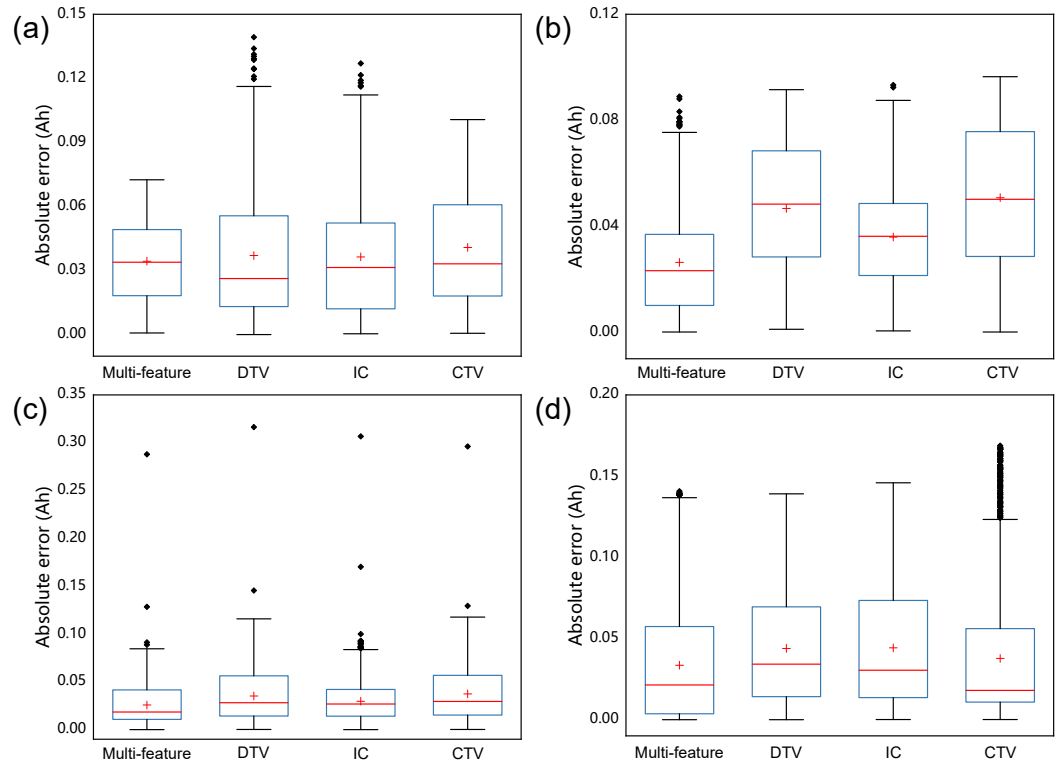


Figure 10. Error plot for different feature extraction methods: (a) $-20\text{ }^{\circ}\text{C}$; (b) $-10\text{ }^{\circ}\text{C}$; (c) $0\text{ }^{\circ}\text{C}$; (d) $25\text{ }^{\circ}\text{C}$.

4.4. Outlook

The proposed MF-TLF marks a significant advancement in LIBs capacity prediction, particularly under small-sample and diverse operational conditions. However, there remain several avenues for further exploration to enhance its robustness, scalability, and practical application. Future research could focus on integrating physics-informed models to complement the data-driven methodology, thereby improving the interpretability and reliability of the predictions. Additionally, incorporating uncertainty quantification and noise-aware techniques would enhance the framework's adaptability to dynamic, real-time environments with noisy data. A hybrid approach that incorporates electrochemical principles alongside transfer learning could provide a more comprehensive understanding of battery degradation mechanisms. To address long-term performance, future work will extend the framework's ability to predict degradation over extended horizons by integrating multi-modal data (e.g., impedance spectroscopy, thermal imaging) and advanced aging models.

Scaling the framework for large-scale applications (e.g., electric vehicle fleets or grid storage) will require optimizations such as distributed data processing, lightweight architectures, and hardware acceleration to ensure efficient edge deployment. Furthermore, expanding the validation to diverse battery chemistries and extreme operational conditions (such as high discharge rates and non-standard charging protocols) will strengthen its generalizability. To ensure feasibility in real-world systems, explainability tools will be integrated to decode the “black-box” nature of data-driven models, providing actionable insights into degradation drivers. Finally, continual learning strategies and adaptive feature engineering will be developed to enable real-time model updates and maintain accuracy under evolving battery technologies, such as solid-state or sodium-ion batteries.

5. Conclusions

This study proposed a multi-feature transfer learning framework (MF-TLF) for accurately predicting lithium-ion battery capacity trajectories under varying operating conditions, especially in small-sample scenarios. The framework integrates a Convolutional Neural Network-Bi-directional Long Short-Term Memory (CNN-BiLSTM)-based transfer learning (TL) model with advanced multi-feature analysis methods to capture critical aging characteristics from temperature, voltage, and current data. The multi-feature analysis approach leverages techniques such as Differential Thermal Voltage (DTV) and Incremental Capacity (IC) analysis to extract comprehensive features representing battery degradation. Additionally, a simple and online-usable Cumulative Thermal Voltage (CTV) method was developed to address the timeliness of feature extraction. The CNN-BiLSTM-based transfer learning model demonstrated robust accuracy and generalization across diverse datasets. In the pretraining phase, the model was trained on data-rich datasets, while in the fine-tuning phase, the BiLSTM block was selectively optimized to adapt to specific degradation patterns under different operating conditions. Extensive experiments were conducted using both the multi-temperature experimental dataset and publicly available datasets. The framework achieved RMSE values below 0.05 Ah, even when using only the first 10% of the target dataset for fine-tuning. These results underscore the method's high accuracy, strong generalization capability, and adaptability to varying conditions. The proposed MF-TLF provides a promising tool for intelligent battery management systems, offering valuable insights and advanced technologies to enhance the reliability and performance of lithium-ion batteries in real-world applications.

Author Contributions: Conceptualization, X.L. and S.C.; data curation, X.G.; formal analysis, X.Y. and S.C.; funding acquisition, Y.S., Y.Y. and X.G.; investigation, Y.S.; methodology, X.Y. and H.X.; project administration, S.C.; resources, X.Y. and Y.Y.; software, X.Y. and J.W.; supervision, S.C.; validation, X.W. and H.X.; visualization, X.W.; writing—original draft, X.L. and X.Y.; writing—review and editing, X.L. and X.Y. All authors have read and agreed to the published version of the manuscript.

Funding: This research is funded by the special cost project of State Grid Jilin Electric Power Company Limited, “research on the state of health estimation of power batteries based on refined battery management”.

Data Availability Statement: The original contributions presented in the study are included in the article, further inquiries can be directed to the corresponding author.

Conflicts of Interest: The authors declare no conflicts of interest.

References

1. Rahman, T.; Alharbi, T. Exploring Lithium-Ion Battery Degradation: A Concise Review of Critical Factors, Impacts, Data-Driven Degradation Estimation Techniques, and Sustainable Directions for Energy Storage Systems. *Batteries* **2024**, *10*, 220. [[CrossRef](#)]
2. Yang, X.; Xie, H.; Zhang, L.; Yang, K.; Liu, Y.; Chen, G.; Ma, B.; Liu, X.; Chen, S. Early-stage degradation trajectory prediction for lithium-ion batteries: A generalized method across diverse operational conditions. *J. Power Sources* **2024**, *612*, 234808. [[CrossRef](#)]
3. Urquiza, J.; Singh, P. A review of health estimation methods for Lithium-ion batteries in Electric Vehicles and their relevance for Battery Energy Storage Systems. *J. Energy Storage* **2023**, *73*, 109194. [[CrossRef](#)]
4. Gao, Z.; Xie, H.; Yang, X.; Niu, W.; Li, S.; Chen, S. The Dilemma of C-Rate and Cycle Life for Lithium-Ion Batteries under Low Temperature Fast Charging. *Batteries* **2022**, *8*, 234. [[CrossRef](#)]
5. Chen, S.; Wei, X.; Zhang, G.; Wang, X.; Zhu, J.; Feng, X.; Dai, H.; Ouyang, M. All-temperature area battery application mechanism, performance, and strategies. *Innovation* **2023**, *4*, 100465. [[CrossRef](#)] [[PubMed](#)]
6. Song, Z.; Dong, T.; Chen, S.; Gao, Z. Bio-Inspired Core–Shell Structured Electrode Particles with Protective Mechanisms for Lithium-Ion Batteries. *Small* **2024**, *21*, 2409310. [[CrossRef](#)]
7. Cui, Y.; Shen, X.; Zhang, H.; Yin, Y.; Yu, Z.; Shi, D.; Fang, Y.; Xu, R. Intrinsic Safety Risk Control and Early Warning Methods for Lithium-Ion Power Batteries. *Batteries* **2024**, *10*, 62. [[CrossRef](#)]

8. Edge, J.S.; O’Kane, S.; Prosser, R.; Kirkaldy, N.D.; Patel, A.N.; Hales, A.; Ghosh, A.; Ai, W.; Chen, J.; Yang, J.; et al. Lithium ion battery degradation: What you need to know. *Phys. Chem. Chem. Phys.* **2021**, *23*, 8200–8221. [[CrossRef](#)]
9. Gao, Z.; Xie, H.; Yang, X.; Wang, W.; Liu, Y.; Xu, Y.; Ma, B.; Liu, X.; Chen, S. SOH estimation method for lithium-ion batteries under low temperature conditions with nonlinear correction. *J. Energy Storage* **2024**, *75*, 109690. [[CrossRef](#)]
10. Che, Y.; Hu, X.; Lin, X.; Guo, J.; Teodorescu, R. Health prognostics for lithium-ion batteries: Mechanisms, methods, and prospects. *Energy Environ. Sci.* **2023**, *16*, 338–371. [[CrossRef](#)]
11. Fahmy, H.M.; Hasanien, H.M.; Alsaleh, I.; Ji, H.; Alassaf, A. State of health estimation of lithium-ion battery using dual adaptive unscented Kalman filter and Coulomb counting approach. *J. Energy Storage* **2024**, *88*, 111557. [[CrossRef](#)]
12. Qiao, J.; Wang, S.; Yu, C.; Yang, X.; Fernandez, C. A chaotic firefly—Particle filtering method of dynamic migration modeling for the state-of-charge and state-of-health co-estimation of a lithium-ion battery performance. *Energy* **2023**, *263*, 126164. [[CrossRef](#)]
13. Lin, C.; Xu, J.; Hou, J.; Liang, Y.; Mei, X. Ensemble Method with Heterogeneous Models for Battery State-of-Health Estimation. *IEEE Trans. Ind. Inform.* **2023**, *19*, 10160–10169. [[CrossRef](#)]
14. Xu, H.; Wu, L.; Xiong, S.; Li, W.; Garg, A.; Gao, L. An improved CNN-LSTM model-based state-of-health estimation approach for lithium-ion batteries. *Energy* **2023**, *276*, 127585. [[CrossRef](#)]
15. Zuo, H.; Liang, J.; Zhang, B.; Wei, K.; Zhu, H.; Tan, J. Intelligent estimation on state of health of lithium-ion power batteries based on failure feature extraction. *Energy* **2023**, *282*, 128794. [[CrossRef](#)]
16. Das, K.; Kumar, R. Electric vehicle battery capacity degradation and health estimation using machine-learning techniques: A review. *Clean Energy* **2023**, *7*, 1268–1281. [[CrossRef](#)]
17. Bockrath, S.; Lorentz, V.; Pruckner, M. State of health estimation of lithium-ion batteries with a temporal convolutional neural network using partial load profiles. *Appl. Energy* **2023**, *329*, 120307. [[CrossRef](#)]
18. Lin, M.; Wu, J.; Meng, J.; Wang, W.; Wu, J. State of health estimation with attentional long short-term memory network for lithium-ion batteries. *Energy* **2023**, *268*, 126706. [[CrossRef](#)]
19. Kopp, M.; Fill, A.; Ströbel, M.; Birke, K.P. A Novel Long Short-Term Memory Approach for Online State-of-Health Identification in Lithium-Ion Battery Cells. *Batteries* **2024**, *10*, 77. [[CrossRef](#)]
20. Madani, S.S.; Ziebert, C.; Vahdatkhah, P.; Sadrnezhaad, S.K. Recent Progress of Deep Learning Methods for Health Monitoring of Lithium-Ion Batteries. *Batteries* **2024**, *10*, 204. [[CrossRef](#)]
21. Yu, H.; Zhang, L.; Wang, W.; Li, S.; Chen, S.; Yang, S.; Li, J.; Liu, X. State of charge estimation method by using a simplified electrochemical model in deep learning framework for lithium-ion batteries. *Energy* **2023**, *278*, 127846. [[CrossRef](#)]
22. Zhang, Z.; Min, H.; Guo, H.; Yu, Y.; Sun, W.; Jiang, J.; Zhao, H. State of health estimation method for lithium-ion batteries using incremental capacity and long short-term memory network. *J. Energy Storage* **2023**, *64*, 107063. [[CrossRef](#)]
23. Zhao, H.; Chen, Z.; Shu, X.; Shen, J.; Lei, Z.; Zhang, Y. State of health estimation for lithium-ion batteries based on hybrid attention and deep learning. *Reliab. Eng. Syst. Saf.* **2023**, *232*, 109066. [[CrossRef](#)]
24. Li, Z.; Zhang, X.; Gao, W. State of health estimation of lithium-ion battery during fast charging process based on BiLSTM-Transformer. *Energy* **2024**, *311*, 133418. [[CrossRef](#)]
25. Zhang, C.; Zhou, Y.; Zhou, Z.; Chen, S.; Wu, J.; Chen, L. State of Health Estimation of Lithium-ion Batteries Based on Multiphysics Features and CNN-EFC-BiLSTM. *IEEE Sens. J.* **2024**, *24*, 39394–39408. [[CrossRef](#)]
26. Fei, Z.; Zhang, Z.; Yang, F.; Tsui, K.-L. A deep attention-assisted and memory-augmented temporal convolutional network based model for rapid lithium-ion battery remaining useful life predictions with limited data. *J. Energy Storage* **2023**, *62*, 106903. [[CrossRef](#)]
27. Lu, J.; Xiong, R.; Tian, J.; Wang, C.; Sun, F. Deep learning to estimate lithium-ion battery state of health without additional degradation experiments. *Nat. Commun.* **2023**, *14*, 2760. [[CrossRef](#)]
28. Liu, S.; Nie, Y.; Tang, A.; Li, J.; Yu, Q.; Wang, C. Online health prognosis for lithium-ion batteries under dynamic discharge conditions over wide temperature range. *eTransportation* **2023**, *18*, 100296. [[CrossRef](#)]
29. Lin, C.; Xu, J.; Mei, X. Improving state-of-health estimation for lithium-ion batteries via unlabeled charging data. *Energy Storage Mater.* **2023**, *54*, 85–97. [[CrossRef](#)]
30. Liu, K.; Peng, Q.; Che, Y.; Zheng, Y.; Li, K.; Teodorescu, R.; Widanage, D.; Barai, A. Transfer learning for battery smarter state estimation and ageing prognostics: Recent progress, challenges, and prospects. *Adv. Appl. Energy* **2023**, *9*, 100117. [[CrossRef](#)]
31. Fu, S.; Tao, S.; Fan, H.; He, K.; Liu, X.; Tao, Y.; Zuo, J.; Zhang, X.; Wang, Y.; Sun, Y. Data-driven capacity estimation for lithium-ion batteries with feature matching based transfer learning method. *Appl. Energy* **2024**, *353*, 121991. [[CrossRef](#)]
32. Yao, J.; Han, T. Data-driven lithium-ion batteries capacity estimation based on deep transfer learning using partial segment of charging/discharging data. *Energy* **2023**, *271*, 127033. [[CrossRef](#)]
33. Chen, J.; Han, X.; Sun, T.; Zheng, Y. Analysis and prediction of battery aging modes based on transfer learning. *Appl. Energy* **2024**, *356*, 122330. [[CrossRef](#)]
34. Zhu, Y.; Shang, Y.; Gu, X.; Wang, Y.; Zhang, C. Rapid assessing cycle life and degradation trajectory based on transfer learning for lithium-ion battery. *IEEE Trans. Transp. Electrif.* **2024**. [[CrossRef](#)]

35. Demirci, O.; Taskin, S.; Schaltz, E.; Acar Demirci, B. Review of battery state estimation methods for electric vehicles-Part II: SOH estimation. *J. Energy Storage* **2024**, *96*, 112703. [[CrossRef](#)]
36. Gupta, A.; Manthiram, A. Designing Advanced Lithium-Based Batteries for Low-Temperature Conditions. *Adv. Energy Mater.* **2020**, *10*, 2001972. [[CrossRef](#)] [[PubMed](#)]
37. Belgibayeva, A.; Rakhmetova, A.; Rakhatkyzy, M.; Kairova, M.; Mukushev, I.; Issatayev, N.; Kalimuldina, G.; Nurpeissova, A.; Sun, Y.-K.; Bakenov, Z. Lithium-ion batteries for low-temperature applications: Limiting factors and solutions. *J. Power Sources* **2023**, *557*, 232550. [[CrossRef](#)]
38. Chen, L.; Bao, X.; Lopes, A.M.; Xu, C.; Wu, X.; Kong, H.; Ge, S.; Huang, J. State of health estimation of lithium-ion batteries based on equivalent circuit model and data-driven method. *J. Energy Storage* **2023**, *73*, 109195. [[CrossRef](#)]
39. Deng, Z.; Xu, L.; Liu, H.; Hu, X.; Duan, Z.; Xu, Y. Prognostics of battery capacity based on charging data and data-driven methods for on-road vehicles. *Appl. Energy* **2023**, *339*, 120954. [[CrossRef](#)]

Disclaimer/Publisher's Note: The statements, opinions and data contained in all publications are solely those of the individual author(s) and contributor(s) and not of MDPI and/or the editor(s). MDPI and/or the editor(s) disclaim responsibility for any injury to people or property resulting from any ideas, methods, instructions or products referred to in the content.